THIELE CENTRE
FOR APPLIED MATHEMATICS IN NATURAL SCIENCE

A Spatio-temporal Model for fMRI Data

Eva B. Vedel Jensen and Thordis L. Thorarinsdottir

Research Report No. 11 | October 2004

A Spatio-temporal Model for fMRI Data

This Thiele Research Report is also Research Report number 449 in the Stochastics Series at Department of Mathematical Sciences, University of Aarhus, Denmark.

A spatio-temporal model for fMRI data

Eva B. Vedel Jensen* Thordis L. Thorarinsdottir*,†

Abstract

Functional magnetic resonance imaging (fMRI) is a technique for studying the active human brain. During the fMRI experiment, a sequence of MR images is obtained, where the brain is represented as a set of voxels. The data obtained are a realization of a complex spatio-temporal process with many sources of variation, both biological and technical. Most current model-based methods of analysis are based on a two-step procedure. The initial step is a voxel-wise analysis of the temporal changes in the data while the spatial part of the modelling is done separately as a second step in the analysis. We present a spatio-temporal point process model approach for fMRI data where the temporal and spatial activation are modelled simultaneously. This modelling framework allows for more flexibility in the experimental design than most standard methods. It is also possible to analyze other characteristics of the data than just the locations of active brain regions, such as the interaction between the active regions. In this paper, we discuss statistical inference in the model based on mean value, variance and covariance. We analyze simulated data without repeated stimuli both for location of the activated regions and for interactions between the activated regions.

1 Introduction

Functional Magnetic Resonance Imaging (fMRI) is a non-invasive imaging technique that has been available for about ten years. Cognitive psychologists and neuroscientists have shown an enormous interest in fMRI because it is believed that fMRI can reveal the human brain in action. There is a comprehensive literature on the topic, mainly in *Human Brain Mapping*, *Magnetic Resonance in Medicine* and *NeuroImage*, reporting various empirical findings and new methods of analysis.

During a typical fMRI experiment, the subject is asked to perform specific behavioral tasks (like finger-tapping or calculations) or the subject is exposed to passive stimulus (like flashing light). The experiment is carefully designed with periods of no specific stimulus ('off periods') between periods of stimuli ('on periods'). The brain is scanned during the experiment and represented as a set of voxels. At each voxel a time series is recorded, showing the local brain activity during the experiment. An informative introduction for statisticians to the design of fMRI experiments can be found in the paper by Genovese (2000).

*The T.N. Thiele Centre, Department of Mathematical Sciences, University of Aarhus.
†The MR Centre, Skejby University Hospital, University of Aarhus

The analysis of fMRI data is usually aimed at localizing the activated or deactivated parts of the brain during the experiment. The initial analysis is often performed voxel-wise, using the time series available at each voxel. The variation in the local signal intensity is analyzed using a temporal model, involving the known design of the experiment and the hemodynamic response function. Using this technique, local activation estimates based on level changes during on and off periods are assessed. Spatial modelling of fMRI data is usually done after the image of voxel-wise activation estimates (for instance an image of $p-$values for activation tested by $t-$tests) is obtained. The most common approach is to use Gaussian random field theory for this part of the modelling, see Friston *et al.* (1995) and Cao and Worsley (1999). The approach is not without problems since the threshold value will depend on the search volume. This type of procedure, involving generalized linear models, has been implemented in the SPM (Statistical Parametric Mapping) software package. The package has been developed by members and collaborators of the Wellcome Department of Imaging Neuroscience, UCL, UK.

In Genovese (2000), a fully Bayesian analysis of fMRI data is discussed, see also Friston (2002), Friston *et al.* (2002a), and Friston *et al.* (2002b). The model still only involves one voxel at a time but is very heavy computationally. In the comments to Genovese (2000), see Worsley (2000), it is suggested to try to spatially link the voxel-wise models. In recent times, ICA (independent component analysis) has become quite popular, cf. Stone (2002) and McKeown *et al.* (2003). See also the early critical comments in Friston (1998). Techniques for detecting functional clusters have been described in Tonini *et al.* (1998).

Especially amongst psychologists there has been some criticism of the localization paradigm. They argue that psychological processes are probably not realized as static constellations. Also, it is believed that the repeated stimulus experiments are artificial. In Greicius *et al.* (2003), the functional connectivity in the resting brain is studied. In particular, the hypothesis of a default mode network is examined. Regions of interest, being deactivated during a cognitive task, are found to be interacting during periods of rest without particular stimulus. This finding is obtained, using an unconventional type of analysis. The average time series from one region is used as an explanatory variable in the analysis of the time variation in other regions of the brain. It is here of interest to try to develop models that can justify this type of data analysis. It is also of interest to find methods for searching for larger clusters showing small magnitudes of activity that are temporally correlated with areas showing large activities.

In a way, these developments are a consequence of the fact that fMRI is a more mature field now. Instead of seeking the locations of active brain regions, the focus is on the interaction between the active regions. This change of paradigm has consequences for the choice of appropriate method of analysis. Instead of looking for changes in level it seems to be more promising to study the covariation between the time series.

A first attempt to provide a modelling framework for experiments without repeated stimuli is outlined in the present paper. Such an experiment will be called a nonstimulus experiment. In our approach the temporal and the spatial part of the activation are modelled simultaneously. We use a high-level model for the spatial

activation and follow the point process approach in Taskinen (2001) and Hartvig (2002), where the spatial activation is modelled using Gaussian bell functions. The model studied in Hartvig (2002) is in its simplest form as follows

$$Z_{tx} = \sum_j h(x - x_j)\varphi_t + \sigma\varepsilon_{tx}$$

where Z_{tx} is the observed MR signal intensity at time t and voxel x, $\{x_j\}$ is a Poisson point process defined on the brain, h is a Gaussian density function with mean 0 and independent components, φ_t is a regression variable, containing information about the repeated stimulus experiment, and $\varepsilon_{tx} \sim N(0,1)$ represents the noise.

For a nonstimulus experiment it seems obvious to replace φ_t with a stationary stochastic process $\{F_t\}$. One possibility is to consider stimuli at random time points such that

$$F_t = \sum_i g(t - t_i),$$

where $\{t_i\}$ is a Poisson point process on the real line and g is a hemodynamic response function. The general model to be described in the present paper is specified, using marked point process theory. The classical repeated stimulus experiments can also be dealt with, using this modelling approach, but this is not our primary objective. Various methods of analyzing the model will be discussed, with increasing degree of computational complexity. Inference based on mean values, variances and covariances is relatively light from a computationally point of view while methods based on complete likelihood or Bayesian methods are more demanding.

In Section 2, the suggested spatio-temporal model is described. Models for the temporal and spatial parts of the activation profile are discussed in Section 3 while first and second order properties of Z_{tx} are expressed in terms of corresponding properties of the underlying spatio-temporal point process in Section 4. In this section, specific point process models are also discussed. Section 5 describes statistical inference based on mean value and covariance relations. A simulation study is presented in Section 6 while future work and perspectives are outlined in Section 7.

2 The spatio-temporal model

Our general model has the form

$$Z_{tx} = \mu_x + \sum_i f_{tx}(t_i, x_i; m_i) + \sigma_x\varepsilon_{tx}, \tag{1}$$

where μ_x is the baseline signal at voxel x and $\Psi = \{[t_i, x_i; m_i]\}$ is a marked spatio-temporal point process on $[0,T] \times \mathcal{X}$ with marks in $\mathcal{M} \subseteq \mathbb{R}^d$. Here, T represents the duration of the fMRI experiment while $\mathcal{X}$ is a bounded subset of $\mathbb{R}^2$ or $\mathbb{R}^3$, representing a two dimensional slice or a three dimensional volume of the brain. Furthermore, ε_{tx} is the error term with $\mathbb{E}\varepsilon_{tx} = 0$ and $\mathbb{V}\varepsilon_{tx} = 1$. It is assumed that $\{\varepsilon_{tx}\}$ are independent of Ψ and that $\{\varepsilon_{tx}\}$ are mutually independent. Various models for correlated noise are discussed in Section 7.

The baseline intensity can vary by an order of magnitude across the volume $\mathcal{X}$. This is due to both variations in the brain tissue as well as variations within the scanner. The baseline μ_x is well determined from data in repeated stimulus experiments and may otherwise be estimated as the value in voxel x in the $T1$ weighted image, which is acquired at the start of each scan (Genovese 2000).

According to (1), the activation profile is described by the marked point process Ψ. Each marked point $[t_i, x_i; m_i]$ may be considered as a centre of activation at location $x_i \in \mathcal{X}$. The centre is activated at time $t_i \in [0, T]$ and its duration and extension are described by the mark $m_i \in \mathcal{M}$. If two regions $\mathcal{X}_0$ and $\mathcal{X}_1$ of the brain interact, it is expected that an activation $[t_{i_0}, x_{i_0}; m_{i_0}]$ in $x_{i_0} \in \mathcal{X}_0$ implies an activation $[t_{i_1}, x_{i_1}; m_{i_1}]$ with t_{i_1} close to t_{i_0} and $x_{i_1} \in \mathcal{X}_1$. Specific point process models with such long-distance-dependencies will be described in Section 4. An illustration of the basic set-up may be found in Figure 1.

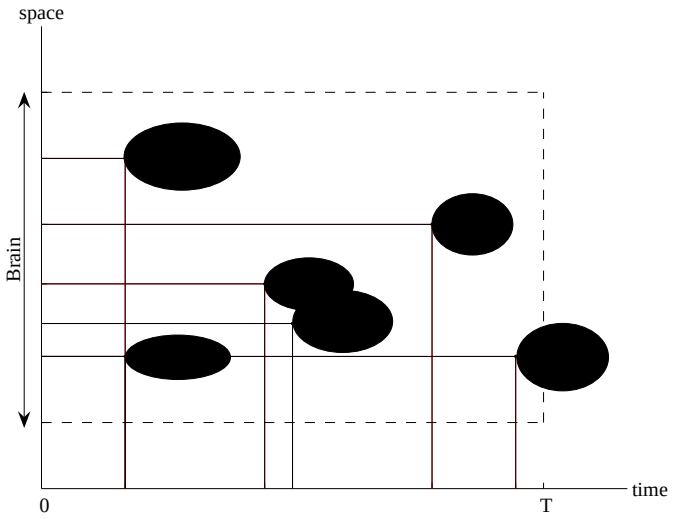

Figure 1: Illustration of the spatio-temporal point process model. Each ellipse illustrates the set of $(t, x) \in \mathbb{R}_+ \times \mathcal{X}$, affected by the activation in the leftmost point (t_i, x_i) of the ellipse. The mark m_i determines the shape and size of the ellipse. In the illustration, an example of simultaneous activation in two different places of the brain is seen, as well as activation of the same place of the brain at different time points.

For modelling of fMRI data, it is interesting to consider an activation profile f_{tx} that can be separated in a temporal and a spatial activation component

$$f_{tx}(u, y; m) = g(t - u; m^1)h(x - y; m^2), \tag{2}$$

where $m = (m^1, m^2) \in \mathcal{M}_1 \times \mathcal{M}_2$ and $\mathcal{M}_i \in \mathbb{R}^{d_i}$, say, $i = 1, 2$. In the fMRI literature, g is called the hemodynamic response function (HRF) and h is the spatial activation function (SAF). The modelling of these two functions will be discussed in the next section.

The standard repeated stimulus experiment can be described within this framework. In such an experiment we have k activation periods with known starting times t_i and known durations l_i, $i = 1, \ldots, k$, cf. Figure 2. Furthermore, let us suppose

that the points $x_j \in \mathcal{X}$ are activated, $j = 1, \ldots, n$. The marked spatio-temporal process then becomes

$$\Psi = \{[t_i, x_j; (m_i^1, m_j^2)]\},$$

where t_i and $m_i^1 = l_i$ are known. In Hartvig (2002), the activation profile is described by

$$\sum_{j=1}^{n} h(x - x_j; m_j^2)\varphi_t,$$

where φ_t is of the form

$$\varphi_t = \int_0^T \pi_u \kappa(t - u)du,$$

$\pi_u = 1$ if $u \in \cup_{i=1}^{k}[t_i, t_i + l_i]$ and κ is the response function for an activation at time 0. This expression can be rewritten as

$$\sum_{i=1}^{k}\sum_{j=1}^{n} f_{tx}(t_i, x_j; m_i^1, m_j^2)$$

where f_{tx} satisfies (2) and

$$g(s; m^1) = \int_0^{m^1} \kappa(s - u)du.$$

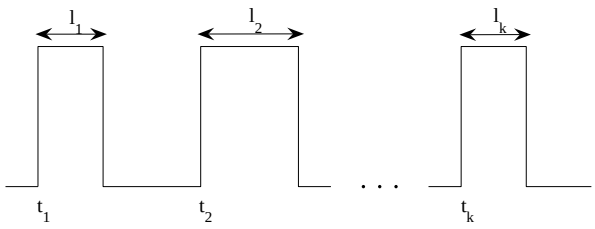

Figure 2: Repeated stimulus experiment.

3 Activation profile

3.1 Temporal activation

Most current fMRI studies rely on the blood oxygenation level dependent (BOLD) effect (Ogawa *et al.* 1992) to detect changes in the MR signal intensity. Neural activity initiates a localized inflow of oxygenated blood to the active area, a *hemodynamic response*. This response is detectable in the MR signal due to different magnetic properties of oxygenated and deoxygenated blood. The biological processes behind the hemodynamic response are not known in detail, but the general structure of the temporal behaviour has been described and reproduced in many studies. The hemodynamic response lags the neuronal activation with several seconds; it increases

slowly to a peak value at about $4-7$ seconds after a neuronal impulse, and then returns to baseline again a few seconds after the neuronal impulse ceases. Often a late undershoot is reported as well, in the sense that when the signal drops after the peak value, it drops below baseline for a period before it returns to the baseline value.

Several different methods for modelling the HRF have been introduced. Perhaps the most precise models are input-state-output models such as the Balloon model (see Buxton *et al.* (2004) and references therein for more details). These models are computationally very complex. The simpler models described below are considered to give a fairly good approximation to empirical studies of the HRF, see Friston *et al.* (1995) and Glover (1999). In these models, g is of the following form

$$g(u; m^1) = \int_0^l \kappa(u - v)du,$$

where l is the temporal duration of the activation. The mark m^1 includes l and possibly other parameters describing the function κ. As discussed above, $\kappa(t) \approx 0$ for $t \leq 0$, κ increases in the interval from 0 to about 4-7 seconds and then decreases to 0, possibly with a drop below 0 before returning to the value 0.

3.1.1 HRF as an integral of Gaussian densities

Based on empirical studies, Friston *et al.* (1995) modelled the delay and dispersion of the hemodynamic response by a Gaussian density with mean 6 sec and variance 9 sec^2 as impulse response. In our formulation, this gives

$$\kappa(t) = \frac{1}{\sqrt{2\pi}3} \exp(-\frac{(t-6)^2}{18}), \tag{3}$$

cf. Figure 3.

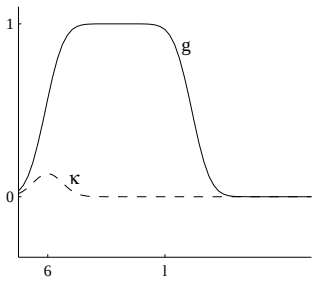

Figure 3: Gaussian response function κ (dashed) and the corresponding integrated response function g (solid).

This model assumes that the temporal activity pattern is the same for all activations during the experiment, which is a rather strong assumption. It is not complicated to make (3) slightly more general, by allowing the mean and the variance of the Gaussian density to vary for each activity. That information would then be included in the mark m^1. The response function would though still not be able to

account for a hemodynamic response with a late undershoot. A natural extension to improve this is to linearly combine (3) with its derivatives with respect to different parameters as in Friston *et al.* (1998).

3.1.2 HRF as an integral of gamma functions

Other empirical studies (Glover 1999) have shown that gamma functions may be more appropriate than Gaussian densities to capture the shape of the HRF. Glover uses the difference of two gamma functions, one to capture the main response and the other to capture the late undershoot. That is, the HRF is modelled by

$$\kappa(t) = \left[\left(\frac{t}{p_1} \right)^{a_1} \exp\left(-\frac{t-p_1}{b_1} \right) - c \left(\frac{t}{p_2} \right)^{a_2} \exp\left(-\frac{t-p_2}{b_2} \right) \right] \mathbb{1}\{t > 0\},$$

where t is the time in seconds and $p_j = a_j b_j$ is the time to the peak. In repeated stimulus experiments, $\kappa(t)$ is then convolved with the time course of the stimuli. This model can be made more flexible by expanding $\kappa(t)$ as a Taylor series and convolve the time course with $-\kappa(t) - t\partial\kappa(t)/\partial t$ instead (Worsley 2000).

In our formulation, this means that the mark m^1 is now given by $m^1 = \{a_1, a_2, b_1, b_2, c, l\}$, where l describes the duration of the activation. The number of unknown parameters in the mark can be reduced by using the results from Glover (1999). For auditory response, the parameters were fit to $a_1 = 6, a_2 = 12, b_1 = b_2 = 0.9$ and $c = 0.35$. Motor response gave the result $a_1 = 5, a_2 = 12, b_1 = 1.1, b_2 = 0.9$ and $c = 0.4$. An example is shown in Figure 4.

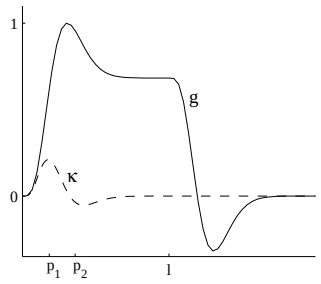

Figure 4: Gamma response function κ (dashed) and the corresponding integrated response function g (solid).

3.2 Spatial activation

The simplest model for the spatial activation is a symmetric Gaussian bell function

$$h(y; m^2) = \theta_1 \exp\left(-\frac{\|y\|^2}{2\theta_2} \right), \tag{4}$$

where $m^2 = (\theta_1, \theta_2)$, $\theta_1, \theta_2 > 0$ and $\|\cdot\|$ is the Euclidean norm in $\mathcal{X}$.

This can be extended as follows. Let $m^2 = (\theta_1, \Theta_2)$ where $\theta_1 > 0$ and Θ_2 is a $p \times p$ positive definite matrix ($p = 2$ or 3). The spatial activation function now

becomes

$$h(y; m^2) = \theta_1 \exp\left(-\frac{1}{2} y^T \Theta_2^{-1} y\right), \tag{5}$$

where y is assumed to be a column vector and $(\cdot)^T$ stands for transpose, see also Hartvig (2002).

32

4 The underlying spatio-temporal point process

In this section, we derive moment relations for the observed MR signal Z_{tx}, under various assumptions on the spatio-temporal point process $\Psi = \{[t_i, x_i; m_i]\}$. The unmarked point process will be denoted by $\Phi = \{[t_i, x_i]\}$. We also discuss specific models for Ψ.

4.1 The mean value relation

We denote the intensity measure for Φ by Λ and let $\Phi(A)$, $A \in \mathcal{B}([0,T] \times \mathcal{X})$, be the number of unmarked points $[t_i, x_i]$ in A. Then,

$$\Lambda(A) = \mathbb{E}\Phi(A).$$

If $\Psi(A \times B)$ denotes the number of marked points $[t_i, x_i; m_i]$ with $[t_i, x_i] \in A$ and $m_i \in B$, $A \in \mathcal{B}([0,T] \times \mathcal{X})$ and $B \in \mathcal{B}(\mathcal{M})$, then the intensity measure of the marked point process is defined by

$$\Lambda_m(A \times B) = \mathbb{E}\Psi(A \times B).$$

Since $\Lambda_m(\cdot \times B) << \Lambda$, there exists for each $(u, y) \in [0,T] \times \mathcal{X}$ a probability distribution $P_{u,y}$ on $(\mathcal{M}, \mathcal{B}(\mathcal{M}))$ such that

$$\Lambda_m(A \times B) = \int_A P_{u,y}(B) \Lambda(du, dy),$$

see also (Stoyan *et al.* 1995, p. 108). Note that $P_{u,y}$ can be interpreted as the distribution of the mark at (u, y). Using the Campbell-Mecke theorem for marked point processes, we find

$$\mathbb{E}Z_{tx} = \mu_x + \int_{[0,T] \times \mathcal{X}} \int_{\mathcal{M}} f_{tx}(u, y; m) P_{u,y}(dm) \Lambda(du, dy).$$

The mean value relation can be further simplified if

$$\Lambda = \Lambda_1 \times \Lambda_2 \tag{6}$$

and

$$P_{u,y} = P_u^1 \times P_y^2. \tag{7}$$

Here, Λ_1 and Λ_2 are measures on $([0,T],\mathcal{B}([0,T]))$ and $(\mathcal{X},\mathcal{B}(\mathcal{X}))$ while P_u^1 and P_y^2 are probability measures on $(\mathcal{M}_1,\mathcal{B}(\mathcal{M}_1))$ and $(\mathcal{M}_2,\mathcal{B}(\mathcal{M}_2))$, respectively. A model satisfying (2), (6) and (7) will be called separable. For a separable model, we have

$$\mathbb{E}Z_{tx} = \mu_x + \alpha_t\beta_x, \tag{8}$$

where

$$\alpha_t = \int_0^T \int_{\mathcal{M}_1} g(t-u;m^1)P_u^1(dm^1)\Lambda_1(du)$$

and

$$\beta_x = \int_{\mathcal{X}} \int_{\mathcal{M}_2} h(x-y;m^2)P_y^2(dm^2)\Lambda_2(dy).$$

The product specification (6) is satisfied for the repeated stimulus experiment described in Section 2. Here, Λ_1 is a discrete measure with weight 1 in $t_i, i = 1,\ldots,k$, and the temporal component of (8) reduces to

$$\alpha_t = \sum_{i=1}^k \int_{\mathcal{M}_1} g(t-t_i;m^1)P_{t_i}^1(dm^1). \tag{9}$$

For the simple response function specified in Section 3.1.1, $P_{t_i}^1$ is concentrated in l_i, the known duration of the ith activation, and

$$\alpha_t = \sum_{i=1}^k g(t-t_i;m_i^1) \tag{10}$$

is known. The mean value specification is a linear regression.

For a nonstimulus experiment, it seems natural to assume that

$$\Lambda = c\nu_T^1 \times \Lambda_2, \tag{11}$$

where $c > 0$ is the temporal intensity of the activations and ν_T^1 is Lebesgue measure on $[0,T]$. Then,

$$\alpha_t = c\int_0^T \int_{\mathcal{M}_1} g(t-u;m^1)P_u^1(dm^1)du.$$

If P_u^1 does not depend on u and the time point t is free of edge affects such that

$$\{u \in \mathbb{R} : g(t-u;m^1) > 0\} \subseteq [0,T],$$

then

$$\begin{aligned}\alpha_t &= c\int_{\mathcal{M}_1}\int_0^T g(t-u;m^1)duP^1(dm^1)\\ &= c\int_{\mathcal{M}_1}\int_{-\infty}^{\infty} g(v;m^1)dvP^1(dm^1)\\ &= c\mathbb{E}\alpha_1(M^1),\end{aligned}$$

where

$$\alpha_1(m^1) = \int_{-\infty}^{\infty} g(v;m^1)dv$$

and M^1 is a random mark, distributed according to P^1. Accordingly, the parameter α_t does not depend on t and the same is true for $\mathbb{E}Z_{tx}$.

4.2 The covariance structure

In contrast to first-order properties, the covariance structure of Z_{tx} depends on the specific choice of point process model. The covariance can be expressed in terms of the so-called second-order factorial moment measure, see Stoyan *et al* (1995, p. 111 and onwards)

Let us here study the case of a marked point process $\Psi = \{[t_i, x_i; m_i]\}$ with conditional independent marks, such that conditionally on $\Phi = \{[t_i, x_i]\}$, $\{m_i\}$ are independent and $m_i \sim P_{t_i,x_i}$. Then,

$$\begin{aligned}
&\mathbb{E}\Big(\sum_{i,i'} f_{tx}(t_i, x_i; m_i) f_{t'x'}(t_{i'}, x_{i'}; m_{i'})\Big) \\
&\quad = \int_{[0,T]\times\mathcal{X}} \int_{\mathcal{M}} f_{tx}(u, y; m) f_{t'x'}(u, y; m) P_{u,y}(dm)\ \Lambda(du, dy) \\
&\qquad + \int_{[0,T]\times\mathcal{X}} \int_{[0,T]\times\mathcal{X}} \int_{\mathcal{M}} \int_{\mathcal{M}} f_{tx}(u, y; m) f_{t'x'}(u', y'; m') P_{u,y}(dm) P_{u',y'}(dm') \\
&\qquad\qquad \times \alpha^{(2)}(du, dy, du', dy'),
\end{aligned}$$

where $\alpha^{(2)}$ is the second-order factorial moment measure for Φ, which is defined for $A, A' \in \mathcal{B}([0, T] \times \mathcal{X})$ by

$$\alpha^{(2)}(A \times A') = \mathbb{E} \sum_{i \neq i'} \mathbb{1}\{[t_i, x_i] \in A, [t_{i'}, x_{i'}] \in A'\}.$$

It follows that

$$\begin{aligned}
&\mathrm{Cov}(Z_{tx}, Z_{t',x'}) \\
&\quad = \int_{[0,T]\times\mathcal{X}} \int_{\mathcal{M}} f_{tx}(u, y; m) f_{t'x'}(u, y; m) P_{u,y}(dm)\ \Lambda(du, dy) \\
&\qquad + \int_{[0,T]\times\mathcal{X}} \int_{[0,T]\times\mathcal{X}} \int_{\mathcal{M}} \int_{\mathcal{M}} f_{tx}(u, y; m) f_{t',x'}(u', y'; m') P_{u,y}(dm) P_{u',y'}(dm') \\
&\qquad\qquad \times [\alpha^{(2)}(du, dy, du', dy') - \Lambda(du, dy)\Lambda(du', dy')] \\
&\qquad + \mathbb{1}\{(t, x) = (t', x')\}\sigma_x^2. \qquad (12)
\end{aligned}$$

The second-order factorial moment measure $\alpha^{(2)}$ is equal to $\Lambda \times \Lambda$ if Φ is a Poisson point process, cf. Stoyan *et al* (1995, p. 44). If

$$\alpha^{(2)}(du, dy, du', dy') - \Lambda(du, dy)\Lambda(du', dy') > 0,$$

then pairs of activations are more likely to occur jointly at (u, y) and (u', y') than for a Poisson point process with intensity measure Λ.

4.3 Specific point process models

In this section, the covariance structure of $\{Z_{tx}\}$ is studied under various types of spatio-temporal point process models.

Example 4.1 (Poisson point process)**.** Suppose that model (1) is satisfied, where $\Phi = \{[t_i, x_i]\}$ is a Poisson point process on $[0,T]\times\mathcal{X}$ with conditionally independent marking. An example is shown in Figure 5, left.

Since $\alpha^{(2)} = \Lambda \times \Lambda$ in this case, we find using (12)

$$\begin{aligned}\operatorname{Cov}\big(Z_{tx}, Z_{t'x'}\big) = &\int_{[0,T]\times\mathcal{X}} \int_{\mathcal{M}} f_{tx}(u,y;m) f_{t'x'}(u,y;m) P_{s,y}(dm)\Lambda(du,dy) \\ &+ \mathbb{1}\{(t,x) = (t',x')\}\sigma_x^2. \end{aligned} \tag{13}$$

For $(t,x) \neq (t',x')$, the correlation between Z_{tx} and $Z_{t'x'}$ becomes

$$\rho(Z_{tx}, Z_{t'x'}) = \frac{I_{tx,t'x'}}{[I_{tx,tx} + \sigma_x^2]^{1/2}[I_{t'x',t'x'} + \sigma_{x'}^2]^{1/2}},$$

where

$$I_{tx,t'x'} = \int_{[0,T]\times\mathcal{X}} \int_{\mathcal{M}} f_{tx}(u,y;m) f_{t'x'}(u,y;m) P_{u,y}(dm)\Lambda(ds,dy).$$

For a separable process ((2), (6) and (7) are satisfied), we get

$$\operatorname{Cov}\left(Z_{tx}, Z_{t'x'}\right) = \rho_{t,t'}\tau_{x,x'} + \mathbb{1}\{(t,x) = (t',x')\}\sigma_x^2,$$

where

$$\rho_{t,t'} = \int_0^T \int_{\mathcal{M}_1} g(t-u;m^1) g(t'-u;m^1) P_u^1(dm^1)\Lambda_1(ds)$$

and

$$\tau_{x,x'} = \int_{\mathcal{X}} \int_{\mathcal{M}_2} h(x-y;m^2) h(x'-y;m^2) P_y^2(dm^2)\Lambda_2(dy).$$

In the case of a nonstimulus experiment with (11) satisfied, we get, if P_u^1 does not depend on u, for time points t, t' free of edge effects

$$\begin{aligned}\rho_{t,t'} &= c\int_0^T \int_{\mathcal{M}_1} g(t-u;m^1) g(t'-u;m^1) P^1(dm^1)du \\ &= c\int_{\mathcal{M}_1} \int_{-\infty}^{\infty} g(t-u;m^1) g(t'-u;m^1) du P^1(dm^1) \\ &= c\int_{\mathcal{M}_1} \int_{-\infty}^{\infty} g(v;m^1) g(v+|t'-t|;m^1) du P^1(dm^1) \\ &= c\mathbb{E}\alpha_2(|t'-t|;M^1),\end{aligned}$$

say, where

$$\alpha_2(t;m^1) = \int_{-\infty}^{\infty} g(v;m^1) g(v+t;m^1) dv$$

and M^1 is a random mark distributed according to P^1. It follows that the covariance between Z_{tx} and $Z_{t'x'}$ depends on t and t' only via $|t-t'|$.

We cannot use this simple Poisson model to describe correlation between distant activation centres. For instance, suppose that

$$h(y; m^2) = \theta_1 \exp\left(-\frac{\|y\|^2}{2\theta_2}\right),$$

where $\theta_1, \theta_2 > 0$. Then, under the assumption that θ_1 and θ_2 do not depend on the location

$$\tau_{x,x'} = \int_{\mathcal{X}} (\theta_1)^2 \exp(-\frac{\|x-y\|^2 + \|x'-y\|^2}{2\theta_2})\Lambda_2(dy). \tag{14}$$

The parameter $\tau_{x,x'}$ will be small if Λ_2 is concentrated around x and x' but the distance between x and x' is large.

In the next two examples, we present point process models that can describe long-distance-dependencies.

Example 4.2 (Independent spatial and temporal point patterns)**.** As before, we consider the model in (1), now with $\Psi = \{[t_i, x_j; m_i^1, m_j^2]\}$. We assume that $\Psi_1 = \{[t_i; m_i^1]\}$ and $\Psi_2 = \{[x_j; m_j^2]\}$ are independent. An example with Ψ_1 and Ψ_2 Poisson is shown in Figure 5, middle.
We assume that (2) is satisfied. Then, since Ψ_1 and Ψ_2 are independent, (6) and (7) also hold and the model is separable. We have

$$Z_{tx} = \mu_x + A_t B_x + \sigma_x \varepsilon_{tx},$$

where

$$A_t = \sum_i g(t - t_i; m_i^1) \text{ and } B_x = \sum_j h(x - x_j; m_j^2) \tag{15}$$

are independent. The covariance is of the form

$$\begin{aligned}\operatorname{Cov}(Z_{tx}, Z_{t'x'}) = \operatorname{Cov}(A_t, A_{t'}) \operatorname{Cov}(B_x, B_{x'}) + \operatorname{Cov}(A_t, A_{t'})\beta_x\beta_{x'} \\ + \alpha_t\alpha_{t'} \operatorname{Cov}(B_x, B_{x'}) + \mathbb{1}\{(t,x) = (t',x')\}\sigma_x^2.\end{aligned}$$

For a repeated stimulus experiment, A_t is deterministic and the expression for the covariance reduces to

$$\operatorname{Cov}(Z_{tx}, Z_{t'x'}) = \alpha_t\alpha_{t'} \operatorname{Cov}(B_x, B_{x'}) + \mathbb{1}\{(t,x) = (t',x')\}\sigma_x^2,$$

where α_t takes the form (9) or (10), depending on the specific assumption on the HRF. If the temporal process $\{t_i\}$ is Poisson and conditionally on $\{t_i\}$, $\{m_i^1\}$ are independent and $m_i^1 \sim P_{t_i}^1$, we get

$$\operatorname{Cov}(A_t, A_{t'}) = \rho_{t,t'}.$$

Similarly, if the spatial process is Poisson with conditionally independent marking

$$\operatorname{Cov}(B_x, B_{x'}) = \tau_{x,x'}.$$

If both processes are Poisson with conditionally independent marking, we thus have

$$\operatorname{Cov}(Z_{tx}, Z_{t'x'}) = \rho_{t,t'}\tau_{x,x'} + \rho_{t,t'}\beta_x\beta_{x'} + \alpha_t\alpha_{t'}\tau_{x,x'} + \mathbb{1}\{(t,x) = (t',x')\}\sigma_x^2.$$

More generally, if both processes $\{t_i\}$ and $\{x_j\}$ have conditionally independent marking, $\{t_i\}$ is Poisson and $\{x_j\}$ is a general point process with second-order factorial moment measure $\alpha^{(2)}$, then

$$\begin{aligned}\operatorname{Cov}(Z_{tx}, Z_{t'x'}) = [\rho_{t,t'} + \alpha_t\alpha_{t'}][\tau_{x,x'} + \delta_{x,x'}] \\ + \rho_{t,t'}\beta_x\beta_{x'} + \mathbb{1}\{(t,x) = (t',x')\}\sigma_x^2,\end{aligned} \tag{16}$$

where

$$\begin{aligned}\delta_{x,x'} = \int_{\mathcal{X}}\int_{\mathcal{X}}\int_{\mathcal{M}_2}\int_{\mathcal{M}_2} h(x-y;m^2)h(x'-y';m^{2'})P_y^2(dm^2)P_{y'}^2(dm^{2'}) \\ \times [\alpha^{(2)}(dy,dy') - \Lambda_2(dy)\Lambda_2(dy')].\end{aligned}$$

Note that $\delta_{x,x'} = 0$ if $\{x_j\}$ is Poisson.

Let us suppose that P_u^1 does not depend on u. For a nonstimulus experiment with (11) satisfied, (16) reduces to the following expression, for time points t, t' free of edge effects,

$$\begin{aligned}\operatorname{Cov}(Z_{tx}, Z_{t'x'}) = c\mathbb{E}\alpha_2(|t'-t|;M^1)[\tau_{x,x'} + \delta_{x,x'} + \beta_x\beta_{x'}] \\ + c^2[\mathbb{E}\alpha_1(M^1)]^2[\tau_{x,x'} + \delta_{x,x'}] + \mathbb{1}\{(t,x) = (t',x')\}\sigma_x^2.\end{aligned} \tag{17}$$

If $\tau_{x,x'}$ is of the form (14), we get for x, x' with large mutual distance for a spatial Poisson process

$$\operatorname{Cov}(Z_{tx}, Z_{t'x'}) \approx c\mathbb{E}\alpha_2(|t'-t|;M^1)\beta_x\beta_{x'}.$$

Example 4.3 (Conditional independent spatial processes)**.** The spatio-temporal process is given by $\Psi = \{[t_i, x_{ij}; m_i^1, m_{ij}^2]\}$. Conditionally on the temporal process $\Psi_1 = \{[t_i; m_i^1]\}$, the spatial processes $\Psi_{2i} = \{[x_{ij}; m_{ij}^2]\}$ are independent and identically distributed with second-order factorial moment measure $\alpha^{(2)}$. It is not difficult to show that if (2) is satisfied, then Ψ is separable.

Under the model of conditional independent spatial processes, the covariance is of the form

$$\begin{aligned}\operatorname{Cov}(Z_{tx}, Z_{t'x'}) = \operatorname{Cov}(A_t, A_{t'})\beta_x\beta_{x'} + \rho_{t,t'}\operatorname{Cov}(B_x, B_{x'}) \\ + \mathbb{1}\{(t,x) = (t',x')\}\sigma_x^2,\end{aligned}$$

with the notation of the previous example. For a repeated stimulus experiment, A_t is deterministic and the expression for the covariance reduces to

$$\operatorname{Cov}(Z_{tx}, Z_{t',x'}) = \rho_{t,t'}\operatorname{Cov}(B_x, B_{x'}) + \mathbb{1}\{(t,x) = (t',x')\}\sigma_x^2.$$

If instead the temporal process is Poisson, the covariance is of the form

$$\operatorname{Cov}(Z_{tx}, Z_{t'x'}) = \rho_{t,t'}[\tau_{x,x'} + \delta_{x,x'} + \beta_x\beta_{x'}] + \mathbb{1}\{(t,x) = (t',x')\}\sigma_x^2, \tag{18}$$

again with the notation of the previous example. An example with Ψ_1 and Ψ_2 Poisson is shown in Figure 5, right.

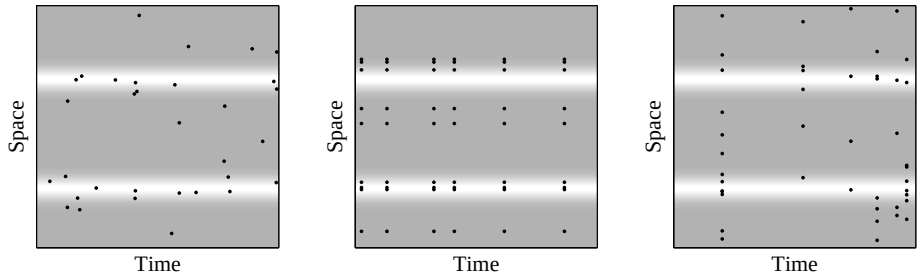

Figure 5: Spatio-temporal Poisson process (left), independent spatial and temporal Poisson processes (middle), and conditionally independent Poisson processes (right). The associated intensity functions are shown in gray scale.

5 Statistical inference

5.1 Spatial smoothing

In the analysis of fMRI data, spatial smoothing is often performed in order to reduce the noise in the data. Suppose the data is smoothed by replacing Z_{tx} with $\tilde{Z}_{tx} = \sum_{z \in \mathcal{X}_x} \omega_{z-x} Z_{tz}$, where $\mathcal{X}_x$ is a neighbourhood around x. We suppose that $\mathcal{X}_x = \mathcal{X}_0 + x$. Furthermore, ω_y, $y \in \mathcal{X}_0$, satisfy $\omega_y \geq 0$ and $\sum_{y \in \mathcal{X}_0} \omega_y = 1$. If $\{Z_{tx}\}$ satisfy (1) and (2), then

$$\tilde{Z}_{tx} = \tilde{\mu}_x + \sum_i \tilde{g}(t - t_i; m_i^1)\tilde{h}(x - x_i; m_i^2) + \tilde{\sigma}_x \tilde{\varepsilon}_{tx}$$

where

$$\tilde{\mu}_x = \sum_{u \in \mathcal{X}_0} \omega_u \mu_{x+u},$$

the function $\tilde{g}$ is simply g,

$$\tilde{h}(v; m^2) = \sum_{u \in \mathcal{X}_0} \omega_u h(v + u; m^2),$$

and

$$\tilde{\sigma}_x^2 = \sum_{u \in \mathcal{X}_0} \omega_u^2 \sigma_{x+u}^2.$$

Our model is therefore closed under smoothing except for the fact that smoothing introduces correlated errors.

5.2 Inference based on the mean value relation

In this subsection, we will discuss within the framework of a separable model as in (2) the estimation of the intensity measure Λ_2 of the spatial point process, using the general mean value relation (8). We will assume that the marks are identical for all points in which case

$$\mathbb{E}Z_{tx} = \mu_x + \alpha_t \beta_x,$$

where

$$\alpha_t = \int_0^T g(t-s; m^1)\Lambda_1(ds)$$

and

$$\beta_x = \int_{\mathcal{X}} h(x-y; m^2)\Lambda_2(dy).$$

We only consider time points free of edge effects.

In what follows, we let $\widetilde{\alpha}_t = \alpha_t$ in a standard experiment (see (10)) while $\widetilde{\alpha}_t = 1$ in a nonstimulus experiment (see (11)). Note that for fixed m^1 the parameters $\widetilde{\alpha}_t$ are known. Likewise, we let $\widetilde{\Lambda}_2 = \Lambda_2$ in a standard experiment and $\widetilde{\Lambda}_2 = c\alpha_1(m^1)\Lambda_2$ in a nonstimulus experiment where

$$\alpha_1(m^1) = \int_{-\infty}^{\infty} g(u; m^1)du.$$

Also, we assume that μ_x is known and we let $\mu_x = 0$. The mean value relation can then be written as

$$\mathbb{E}Z_{tx} = \widetilde{\alpha}_t\widetilde{\beta}_x,$$

where

$$\widetilde{\beta}_x = \int_{\mathcal{X}} h(x-y; m^2)\widetilde{\Lambda}_2(dy).$$

We will consider the estimation of Λ_2 (or equivalently $\widetilde{\Lambda}_2$) under the assumption that Λ_2 is a discrete measure concentrated in $x_j, j = 1, \ldots, N$, with masses $\lambda_2(x_j) = \Lambda_2(\{x_j\})$, $j = 1, \ldots, N$. Let us suppose that we have discretely observed data in time with spacing Δ

$$\{Z_{i\Delta,x} : i = i_0 + 1, \ldots, i_0 + n, x \in \mathcal{X}\},$$

where all time points are free of edge effects. A simple estimation procedure is to estimate $\widetilde{\beta}_x$ by the regression estimate

$$\widetilde{Z}_x = \sum_{i=1}^{n} \widetilde{\alpha}_{(i_0+i)\Delta} Z_{(i_0+i)\Delta,x} / \sum_{i=1}^{n} \widetilde{\alpha}^2_{(i_0+i)\Delta}$$

and for each m^1 and m^2 minimize

$$\sum_{i=1}^{N}\Big[\widetilde{Z}_{x_i} - \sum_{j=1}^{N} h(x_i - x_j; m^2)\widetilde{\lambda}_2(x_j)\Big]^2 \tag{19}$$

with respect to $\{\widetilde{\lambda}_2(x_j)\}$, subject to the condition $\widetilde{\lambda}_2(x_j) \geq 0$ for all j. Note that in a nonstimulus experiment, Λ_2 and c cannot be separated, using this estimation procedure.

The variance of $\widetilde{Z}_x$ may, however, depend on x. As an example, let us consider a repeated stimulus experiment with Poisson distributed activation centres as described in Example 4.2. Then,

$$\mathbb{V}\widetilde{Z}_x = \tau_{x,x} + \frac{1}{\sum_1^n \alpha^2_{(i_0+i)\Delta}}\sigma_x^2.$$

An unbiased estimate of σ_x^2 is

$$\hat{\sigma}_x^2 = \frac{1}{n-1}\sum_{i=1}^{n}(Z_{(i_0+i)\Delta,x} - \alpha_{(i_0+i)\Delta}\widetilde{Z}_x)^2.$$

Furthermore, a discretized version of $\tau_{x,x}$ is

$$\tau_{x,x} = \sum_{j=1}^{N} h(x - x_j; m^2)^2 \lambda_2(x_j).$$

The unweighted sum of squares may then be replaced by

$$\sum_{i=1}^{N}\Big[\widetilde{Z}_{x_i} - \sum_{j=1}^{N} h(x_i - x_j; m^2)\lambda_2(x_j)\Big]^2 / \mathbb{V}\widetilde{Z}_{x_i},$$

where we insert the derived form of $\mathbb{V}\widetilde{Z}_{x_i}$ and the estimate $\hat{\sigma}_{x_i}^2$. This sum of squares should be minimized with respect to λ_2 for fixed m^1 and m^2.

As another example, let us consider a nonstimulus experiment with independent temporal and spatial Poisson point processes. Then, $\widetilde{Z}_x = \bar{Z}_{\cdot x}$ and, using (17) with $\delta_{x,x'} = 0$, we find

$$\begin{aligned}\mathbb{V}\bar{Z}_{\cdot x} = {} & \frac{c}{n^2}\Big[n\alpha_2(0; m^1) + 2\sum_{i=1}^{n-1}(n-i)\alpha_2(i\Delta; m^1)\Big]\left[\tau_{x,x} + \beta_x^2\right] \\ & + c^2\alpha_1(m^1)^2\tau_{x,x} + \frac{1}{n}\sigma_x^2.\end{aligned}$$

The empirical variance

$$\hat{\sigma}_{x,x} = \frac{1}{n-1}\sum_{i=1}^{n}(Z_{(i_0+i)\Delta,x} - \bar{Z}_{\cdot x})^2$$

can be used to estimate σ_x^2 but the situation is now more complicated.

Generally, if $\mathrm{Cov}(Z_{tx}, Z_{tx'})$ only depend on t and t' via $|t - t'|$,

$$\mathrm{Cov}(Z_{tx}, Z_{t',x'}) = \sigma_{x,x'}(|t - t'|),$$

say, then $\sigma_{x,x'} = \sigma_{x,x'}(0)$ can be estimated by

$$\hat{\sigma}_{x,x'} = \frac{1}{n-1}\sum_{i=1}^{n}(Z_{(i_0+i)\Delta,x} - \bar{Z}_{\cdot x})(Z_{(i_0+i)\Delta,x'} - \bar{Z}_{\cdot x'}), \tag{20}$$

where

$$\bar{Z}_{\cdot x} = \frac{1}{n}\sum_{i=1}^{n} Z_{(i_0+i)\Delta,x}.$$

This estimate is, however, biased because of correlations inside the time series. We thus have

$$\mathbb{E}(\hat{\sigma}_{x,x'}) = \sigma_{x,x'} - \frac{2}{n(n-1)}\sum_{i=1}^{n-1}(n-i)\sigma_{x,x'}(i\Delta). \tag{21}$$

Using (17), (20) and (21), we find that

$$\mathbb{E}(\hat{\sigma}_{x,x}) = c\Big[\alpha_2(0;m^1) - \frac{2}{n(n-1)}\sum_{i=1}^{n-1}(n-i)\alpha_2(i\Delta;m^1)\Big]\left[\tau_{x,x}+\beta_x^2\right] + \sigma_x^2.$$

The variance of $\bar{Z}_{\cdot x}$ can therefore be written as

$$\mathbb{V}\bar{Z}_{\cdot x} = \frac{1}{n}\mathbb{E}(\hat{\sigma}_{x,x}) + c^2\alpha_1(m^1)^2\tau_{x,x} + \frac{2c}{n(n-1)}\sum_{i=1}^{n-1}(n-i)\alpha_2(i\Delta;m^1)[\tau_{x,x}+\beta_x^2].$$

The unweighted sum of squares may be replaced by

$$\sum_{i=1}^{N}\Big[\bar{Z}_{\cdot x_i} - c\alpha_1(m^1)\sum_{j=1}^{N}h(x_i-x_j;m^2)\lambda_2(x_j)\Big]^2 \Big/ \mathbb{V}\bar{Z}_{\cdot x_i}$$

and minimized with respect to $\{\lambda_2(x_j)\}$ for each fixed c, m^1 and m^2.

5.3 Inference based on covariances

In Greicius *et al.* (2003), the average time series from one brain region is used as explanatory variable in the analysis of the time variation in other regions of the brain. This type of analysis can be justified within the modelling framework of the present paper.

Let us concentrate on the conditional independent processes, presented in Example 4.3. Let us consider a nonstimulus experiment, with a Poisson process as temporal process and let the marks be identical for all points. For time points t, t' free of edge effects, we then have, cf. (18),

$$\begin{aligned}\mathrm{Cov}(Z_{tx}, Z_{t',x'}) = {} & c\mathbb{E}\alpha_2(|t'-t|;M^1) \\ & \times\Big[\tau_{x,x'} + \int_{\mathcal{X}}\int_{\mathcal{X}} h(x-y;m^2)h(x'-y';m^2)\alpha^{(2)}(dy,dy')\Big] \\ & + \mathbb{1}\{(t,x)=(t',x')\}\sigma_x^2.\end{aligned}$$

In particular, if $\tau_{x,x'}$ is of the form (14), we get for x, x' with large mutual distance

$$\mathrm{Cov}(Z_{tx}, Z_{t',x'}) \approx c\mathbb{E}\alpha_2(0;M^1)\int_{\mathcal{X}}\int_{\mathcal{X}} h(x-y;m^2)h(x'-y';m^2)\alpha^{(2)}(dy,dy').$$

The slope of the regression of $Z_{t,x'}$ on Z_{tx},

$$\mathrm{Cov}(Z_{tx}, Z_{tx'})/\mathbb{V}Z_{tx},$$

is thus for fixed x and varying x' proportional to

$$\int_{\mathcal{X}}\int_{\mathcal{X}} h(x-y;m^2)h(x'-y';m^2)\alpha^{(2)}(dy,dy').$$

If $h(u;m^2)$ is concentrated around $u=0$, a plot of the slopes will reveal $x' \in \mathcal{X}$ for which $\alpha^{(2)}(dx,dx')$ is large. Recall that $\alpha^{(2)}(dx,dx')$ can be interpreted as the probability of having simultaneously an activation at x and x'.

6 A simulation study

We have simulated data from the model in (1) with independent spatial and temporal Poisson point patterns as in Example 4.2. The object of the simulation study was the analysis of a nonstimulus experiment. Thus, we gave the temporal intensity function a constant value, $\lambda_1(t) = c$ for all $t \in [0, 100]$, while the spatial activation pattern comprised activated areas of various sizes, shapes and peak intensity. The HRF was given by an integral (sum) of Gaussian densities as in Section 3.1.1 with $m^1 = l = 5$ and the spatial activation was modelled by a symmetric Gaussian bell function as in Section 3.2 with $m^2 = (\theta_1, \theta_2) = (4, 4)$. Further, the errors were standard Gaussian distributed, $\varepsilon_{tx} \sim \mathcal{N}(0, 1)$, and we set σ_x^2 to be equal to 10% of the baseline signal.

The activation pattern is shown in Figure 6, with the realization of the temporal activity left and the arranged spatial activity right. Two time series from the simulation are shown in Figure 7, one is from an activated area and one from an area with no activation. The activity pattern in the former clearly follows the temporal activity pattern shown in Figure 6 (left). Figure 8 shows the development of the activity over time. The upper left figure shows the activity at time $t = 10$, the upper middle figure shows the activity at time $t = 20$, and so on.

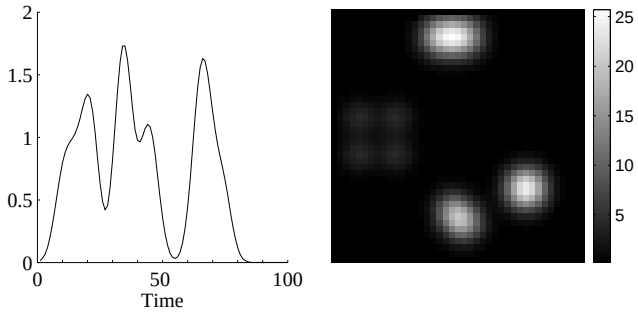

Figure 6: The realization of the temporal activity used in the simulation (left) and the spatial activity (right). The HRF was modelled by a sum of Gaussian functions with mark $m^1 = 5$ and the SAF was modelled by a Gaussian bell function with $m^2 = (4, 4)$. See the main text for more details.

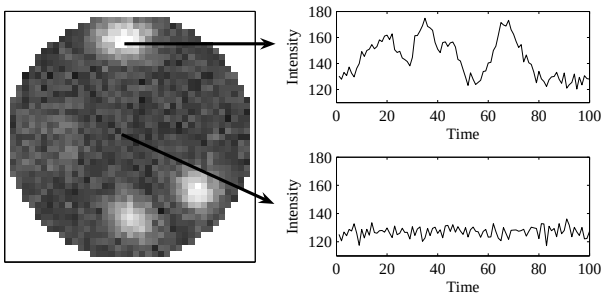

Figure 7: Illustration of time series data from the simulation. Left: simulated data at time $t = 20$. Right: time series of respectively an active (top) and a nonactive (bottom) voxel.

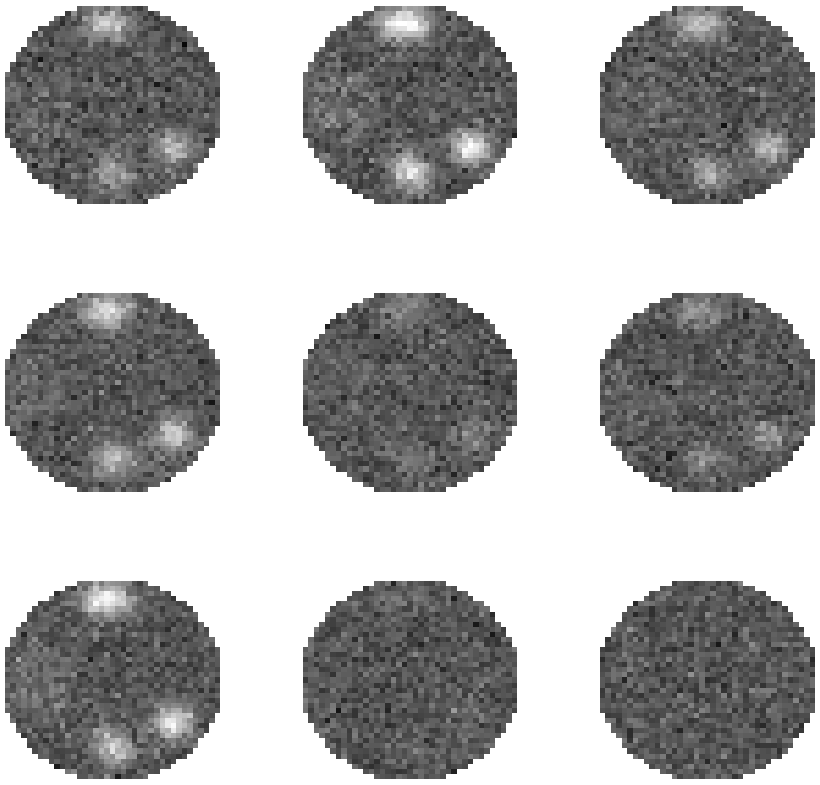

Figure 8: Development of the activity over time. From left to right and top to bottom: the activity at time $t = 10, 20, \ldots, 90$.

We have estimated the spatial intensity function λ_2, using two different methods. In Section 6.1, we used the method based on the general mean value relation as described in Section 5.2. In Section 6.2, we assumed one of the activated areas, $\mathcal{X}_0 \subset \mathcal{X}$, to be known and we searched for other areas in $\mathcal{X}$, functionally connected to $\mathcal{X}_0$. That is, we estimated λ_2 in $\mathcal{X} \setminus \mathcal{X}_0$ using covariances. This method is similar to the inference discussed in Section 5.3.

6.1 Estimation of λ_2 using mean value relations

We used the method described in Section 5.2 with a slight change, as not all the time points in the simulation were free of edge effects. Following the notation in Section 5.2, we let

$$\tilde{\alpha}_t = \int_0^T g(t - s; m^1) ds$$

and

$$\tilde{\Lambda}_2 = c\Lambda_2.$$

The parameter $\tilde{\alpha}_t$ is still known, but depends on t (the dependence is only slight for t near the endpoints of the interval $[0, 100]$). We then continued as described in Section 5.2 and for fixed m^1 and m^2, we minimized (19).

This method gave us an estimate $\hat{\lambda}_2$ of λ_2 up to a constant of proportionality. We scaled $\hat{\lambda}_2$ such that $0 \leq \hat{\lambda}_2(x_i) \leq 1$ for all $i = 1, \ldots, N$, with x_i being the midpoint of each voxel (pixel). Each point x_i was defined to be an activity centre if $r_i < \hat{\lambda}_2(x_i)$, where $r_i \sim \mathcal{U}([0, 1])$, $i = 1, \ldots, N$. The spatial activity was then constructed by placing Gaussian bell functions on top of each activity centre. In order to eliminate outliers, we constructed 100 such activation patterns and used the mean value of these as our estimate for the spatial activation pattern. Figure 9 shows the estimated activation pattern for $m^1 = 5$ and $m^2 = (4, 4)$ (right) together with the true activation pattern (left). The method gives an estimate of the correct activation pattern, up to multiplication with a constant.

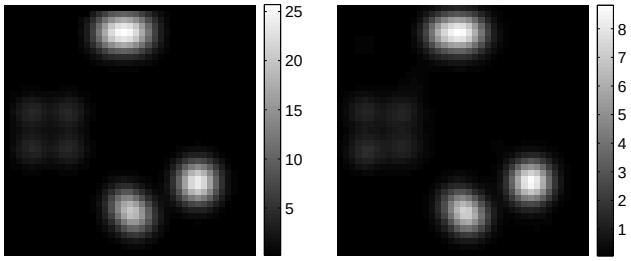

Figure 9: The true spatial activation pattern (left) and the estimated spatial activation pattern (right) with marks $m^1 = 5$ and $m^2 = (4, 4)$.

In order to test the sensitivity of the method towards changes in the marks, we minimized (19) for different values of m^1 and m^2. To make the estimated patterns comparable, we rescaled each estimated spatial activation pattern so that the maximum peak intensity for each estimate coincided with the maximum peak intensity of the true activation pattern. Table 1 shows the L^2-distances between the estimates and the true values, $\|\hat{B} - B\| = \left(\sum_{i=1}^{N} (\hat{B}_{x_i} - B_{x_i})^2\right)^{1/2}$, for different values of m^1 and m^2. Here, B_x is the intensity of the true activation pattern at voxel x and $\hat{B}_x$ the rescaled estimated intensity.

6.2 Estimation of λ_2 using covariances

For data under the model used in the simulation we have, cf. (17),

$$\begin{aligned}\mathrm{Cov}(Z_{tx}, Z_{tx'}) = c\alpha_2(0; m^1) & \\ \times \left[\tau_{x,x'} + \int_{\mathcal{X}} \int_{\mathcal{X}} h(x - y; m^2) h(x' - y'; m^2) \Lambda_2(dy) \Lambda_2(dy')\right] & \\ + c^2 \alpha_1(m^1)^2 \tau_{x,x'} + \mathbb{1}\{x = x'\} \sigma_x^2, &\end{aligned}$$

for a time point t free of edge effects and fixed marks $m = (m^1, m^2)$. In particular, as $\tau_{x,x'}$ is of the form (14), we get for x, x' with large mutual distance

$$\mathrm{Cov}(Z_{tx}, Z_{tx'}) \approx c\alpha_2(0; m^1) \int_{\mathcal{X}} \int_{\mathcal{X}} h(x - y; m^2) h(x' - y'; m^2) \Lambda_2(dy) \Lambda_2(dy').$$

Table 1: L^2-distances between the true spatial activation pattern and the rescaled estimated spatial activation for different values of $m^1 = l$ and $m^2 = (\theta_1, \theta_2)$. The data set has $N = 1681$ voxels.

l	θ_1	θ_2	$\|\hat{B} - B\|$
5	4	4	15.5493
2	4	4	16.8920
8	4	4	14.4175
5	2	4	15.4486
5	6	4	15.8929
5	4	2	14.9534
5	4	6	26.8073

We thus get, as in Section 5.3, that the slope of the regression of $Z_{tx'}$ on Z_{tx},

$$\mathrm{Cov}(Z_{tx}, \mathbb{Z}_{tx'})/\mathbb{V}Z_{tx},$$

is for fixed x and varying x' proportional to

$$\int_{\mathcal{X}} \int_{\mathcal{X}} h(x - y; m^2) h(x' - y'; m^2) \Lambda_2(dy) \Lambda_2(dy'),$$

Assume we have given an activated area, $\mathcal{X}_0$, in $\mathcal{X}$ and wish to find other areas with functional connection to $\mathcal{X}_0$. Based on the calculations above, it is thus reasonable to search for these areas using analysis based on covariances. Figure 10 shows the slope of the regression of $Z_{tx'}$ on Z_{tx} for the simulated data, where x is the point in $\mathcal{X}$ with maximum intensity.

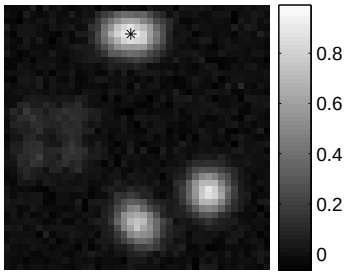

Figure 10: The slope of the regression of $Z_{tx'}$ on Z_{tx} for a fixed point $x \in \mathcal{X}$ and all $x' \in \mathcal{X}$. The point x, shown as a star in the figure, is the point in $\mathcal{X}$ with maximum intensity.

Under the independent Poisson model, used in the simulation, we can also estimate the spatial activation, using the covariances. It follows from (17), (20) and (21), that the mean value of the empirical covariance estimate (20) is given by

$$\mathbb{E}(\hat{\sigma}_{x,x'}) = c\gamma(m^1) \left[\tau_{x,x'} + \beta_x \beta_{x'}\right] + \mathbb{1}\{x = x'\}\sigma_x^2,$$

where

$$\gamma(m^1) = \alpha_2(0; m^1) - \frac{2}{n(n-1)} \sum_{i=1}^{n-1} (n - i) \alpha_2(i\Delta; m^1),$$

for time points t free of edge effects and fixed marks $m = (m^1, m^2)$, as before. As $\tau_{x,x'}$ is of the form (14), we get for x, x' with large mutual distance

$$\mathbb{E}(\hat{\sigma}_{x,x'}) \approx c\gamma(m^1)\beta_x\beta_{x'}.$$

Assume that an activity centre $\mathcal{X}_0 \subset \mathcal{X}$ with N_0 points is known. Then, for x' with large mutual distance from all points $x \in \mathcal{X}_0$,

$$\mathbb{E}\Big(\frac{1}{N_0}\sum_{x\in\mathcal{X}_0}\hat{\sigma}_{x,x'}\Big) \approx c\gamma(m^1)\bar{\beta}_\cdot \sum_{i=1}^{N} h(x' - x_i; m^2)\lambda_2(x_i), \tag{22}$$

where

$$\bar{\beta}_\cdot = \frac{1}{N_0}\sum_{x\in\mathcal{X}_0}\beta_x.$$

This expression is linear in λ_2 if we regard $\bar{\beta}_\cdot$ as an unknown constant. We can thus use least squares methods to estimate $\lambda_2(x)$ for $x \in \mathcal{X} \setminus \mathcal{X}_0$ up to a constant, as in the previous section.

We supposed the upper middle activity centre in Figure 6 (right) to be known. We then used (22) to obtain an estimate $\hat{\lambda}_2(x)$ of $\tilde{\lambda}_2(x) = c\gamma(m^1)\bar{\beta}_\cdot\lambda_2(x)$ for all $x \in \mathcal{X} \setminus \mathcal{X}_0$. Given the estimate of the spatial intensity function, the spatial activity was reconstructed as in the previous section. The results for $m^1 = 5$ and $m^2 = (4, 4)$ are shown in Figure 11. As before, the method finds the correct activation areas, but the intensities are only kown up to a multiplication with a constant.

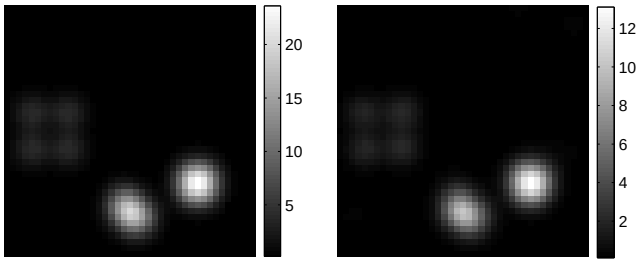

Figure 11: The true spatial activation pattern (left) and the estimated spatial activation pattern (right) for the marks $m^1 = 5$ and $m^2 = (4, 4)$. The upper middle activity centre in Figure 6, denoted by $\mathcal{X}_0$ in the text above, is not shown, as it is assumed known and thus not estimated.

As in the previous section, we have tested the sensitivity of the method towards changes in the marks. The procedure is the same as before, except that here, we only tested for sensitivity towards changes in m^2. Changes in the mark m^1 will only influence the factor γ in (22). Table 2 shows the resulting distance for different values of m^2. Note that the results can not be directly compared to the results in Table 1 since we only consider estimation of the spatial activation for points in $\mathcal{X} \setminus \mathcal{X}_0$.

Table 2: L^2-distances between the true spatial activation pattern and the rescaled estimated spatial activation for different values of $m^1 = l$ and $m^2 = (\theta_1, \theta_2)$. The data set $\mathcal{X} \setminus \mathcal{X}_0$ has $N - N_0 = 1516$ data points.

l	θ_1	θ_2	$\|\hat{B} - B\|$
5	4	4	10.1205
5	2	4	6.7982
5	6	4	9.7661
5	4	2	10.6322
5	4	6	20.0038

7 Discussion

In fMRI experiments, data may have a more complicated structure than the one predicted by our model, cf. e.g. Hartvig (2002). An extended model will most likely include a drift component d_{tx}

$$Z_{tx} = \mu_x + d_{tx} + \sum_i f_{tx}(t_i, x_i; m_i) + \sigma_x \varepsilon_{tx}, \tag{23}$$

cf. Genovese (2000). This component describes the slow drifts in the static magnetic field during the experiment and residual motion not accounted for by prior motion correction. Often, the drift is removed using filtering, before any further analysis of the data, cf. Friston *el al.* (2000), or included in a general linear model, cf. Friston *et al.* (1995). It should also be part of an initial analysis to examine whether the data should be transformed. In Hartvig (2002), log-transformed signal intensities are analyzed by a model as in (23) with $\sigma_x^2 = \sigma^2$. Note that the variance of the untransformed intensities will then depend on t and x.

In the present paper we have mainly used the simple model described in Section 3.1.1 for the temporal activity, one reason being that we want to focus on the spatial modelling. In Genovese (2000), models for the HRF are reviewed, including a model based on splines. In Purdon *et al.* (2001), a new model for a physiologically based hemodynamic response is described.

We have assumed that the errors $\{\varepsilon_{tx}\}$ are mutually independent. It is here important to consider more general error models. In particular, the noise is often autocorrelated in time, as emphasized in Worsley (2000). In Hartvig (2002), a separable covariance structure is described. Let $\varepsilon = \{\varepsilon_{tx} : t = 1, \ldots, T, x \in \mathcal{X}\}$ be the noise term in (23) regarded as a $\mid \mathcal{X} \mid \times T$ matrix. Then,

$$\varepsilon \sim N_{|\mathcal{X}| \times T}(0, \sigma^2 \Gamma \otimes \Xi), \tag{24}$$

where $\otimes$ denotes the Kronecker product and where Γ and Ξ are $\mid \mathcal{X} \mid \times \mid \mathcal{X} \mid$ and $T \times T$ correlation matrices. For each data set, it is then possible to fit an ARMA model to the empirical temporal and spatial correlations separately. However, data analysis suggests that a model with a non-separable covariance structure is more appropriate (Hartvig 1999). One such model is that proposed by Lange and Zeger (1997), where the voxel time series are considered in the frequency domain, and

different spatial covariance models are fitted to different frequencies. Such a noise model increases the computational complexity substantially.

It still remains to study more systematically explicit point process models that can describe how activities in different regions af the brain are related (serially, in parallel). In particular, it is of interest to include time delays in the modelling. For modelling the spatial point process $\{x_i\}$, Taskinen (2001) has suggested a cluster point process. Note also that the point process term

$$\sum_i f_{tx}(t_i, x_i; m_i)$$

of (23) has the form of the random intensity field of a shot noise Cox process if Ψ is Poisson, see e.g. Møller (2003).

From an applied point of view, an important next step is to design nonstimulus experiments along the lines described in Greicius *et al.* (2003) and analyze the data, using the modelling framework presented in this paper. Note that in contrast to the method described in Hartvig (2002), we aim at estimating the intensity surface rather than actually finding the positions of the activation centres.

The statistical analysis described in the present paper, based on mean value and covariance relations, is not very demanding from a computational point of view. It is of interest to study inference based on the complete likelihood. With a specific model for the errors ε and the point process of activations Ψ, the joint density of the MR intensities Z and the point process Ψ can be derived, using that

$$p(z, \psi) = p(z|\psi)p(\psi).$$

Since Ψ is not observed, this is a missing data problem. The marginal density of Z

$$p(z) = \mathbb{E}p(z, \Psi)$$

can be found, using Monte Carlo methods. For more details, see Møller and Waagepetersen (2004, Section 8.6).

Acknowledgements

This work was supported by the Danish Natural Science Research Council. The authors are grateful for fruitful discussions with Klaus B. Bærentsen, Anders Green and Hans Stødkilde-Jørgensen.

References

Buxton, R.B., Uludağ, K., Dubowitz, D.J., and Liu, T.T. (2004): Modelling the hemodynamic response to brain activation. *NeuroImage* **23** S220-S233.

Cao, J. and Worsley, K. (1999): The geometry of correlation fields with an application to functional connectivity of the brain. *The Annals of Applied Probability* **9** 1021-1057.

Friston, K.J. (1998): Modes or models: a critique on independent component analysis for fMRI. With discussion. *Trends in Cognitive Sciences* **2** 373-375.

Friston, K.J. (2002): Bayesian estimation of dynamical systems: an application to fMRI. *NeuroImage* **16** 513-530.

Friston, K.J., Flecther, P., Josephs, O., Holmes, A., Rugg, M.D., and Turner, R. (1998): Event-related fMRI: characterizing differential responses. *NeuroImage* **7** 30-40.

Friston, K.J., Glaser, D.E., Henson, R.N.A., Kiebel, S., Phillips, C., and Ashburner, J. (2002b): Classical and Bayesian inference in neuroimaging: applications. *NeuroImage* **16** 484-512.

Friston, K.J., Holmes, A.P., Poline, J.-B., Grasby, P.J., Williams, S.C.R., Frackowiak, R.S.J., and Turner, R. (1995): Analysis of fMRI time-series revisited. *NeuroImage* **2** 45-53.

Friston, K.J., Josephs, O., Zarahn, E., Holmes, A.P., Rouquette, and Poline, J.-B. (2000): To smooth or not to smooth? *NeuroImage* **12** 196-208.

Friston, K.J., Penny, W., Philips, C., Kiebel, S., Hinton, G., and Ashburner, J. (2002a): Classical and Bayesian inference in neuroimaging: theory. *NeuroImage* **16** 465-483.

Genovese, C.R. (2000): A Bayesian time-course model for functional magnetic resonance imaging data. With discussion and a reply by the author. *Journal of the American Statistical Association* **95** 691-719.

Glover, G.H. (1999): Deconvolution of impulse response in event related fMRI. *NeuroImage* **9** 416-429.

Greicius, M.D., Krasnow, B., Reiss, A.L., and Menon, V. (2003): Functional connectivity in the resting brain: a network analysis of the default mode hypothesis. *Proceedings of the National Academy of Sciences USA* **100** 253-258.

Hartvig, N.V. (1999): A stochastic geometry model for fMRI data. Research Report 410, Department of Theoretical Statistics, University of Aarhus.

Hartvig, N.V. (2000): Parametric modelling of functional magnetic resonance imaging data. PhD thesis, Department of Theoretical Statistics, University of Aarhus.

Hartvig, N.V. (2002): A stochastic geometry model for functional magnetic resonance images. *Scandinavian Journal of Statistics* **29** 333-353.

Lange, N. and Zeger, S.L. (1997): Non-linear Fourier time series analysis for human brain mapping by functional magnetic resonance imaging. With discussion and a reply by the author. *Journal of the Royal Statistical Society, Series C (Applied Statistics)* **46** 1-29.

McKeown, M.J., Hansen, L.K., and Sejnowski, T.J. (2003): Independent component analysis of functional MRI: what is signal and what is noise? *Current Opinion in Neurobiology* **13** 620-629.

Møller, J. (2003): Shot noise Cox processes. *Advances in Applied Probability* **35** 614-640.

Møller, J. and Waagepetersen, R.P. (2004): *Statistical Inference and Simulation for Spatial Point Processes*, Chapman & Hall/CRC, New York.

Ogawa, S., Tank, D.W., Menon, R., Ellermann, J.E., Kim, S., Merkle, H., and Ugurbil, K. (1992): Intrinsic signal changes accompanying sensory stimulation: functional brain mapping with magnetic resonance imaging. *Proceedings of the National Academy of Sciences USA* **89** 5951-5955.

Purdon, P.L., Solo, V., Weisskoff, R.M., and Brown, E.N. (2001): Locally regularized spatiotemporal modeling and model comparison for functional MRI. *NeuroImage* **14** 912-923.

Stone, J.V. (2002): Independent component analysis: an introduction. *Trends in Cognitive Sciences* **6** 59-64.

Stoyan, D., Kendall, W.S., and Mecke, J. (1995): *Stochastic Geometry and Its Applications*, second edn. John Wiley & Sons, Chichester.

Taskinen, I. (2001): Cluster priors in the Bayesian modelling of fMRI data. *PhD Thesis*. Department of Statistics, University of Jyväskylä, Jyväskylä.

Tonini, G., McIntosh, A.R., Russell, D.P., and Edelman, G.M. (1998): Functional clustering: identifying strongly interactive brain regions in neuroimaging data. *NeuroImage* **7** 133-149.

Worsley, K.J. (2000): Comment on *A Bayesian time-course model for functional magnetic resonance imaging* by C. Genovese. *Journal of the American Statistical Association* **95** 691-719.